ACS OMEGA

http://pubs.acs.org/journal/acsodf

Article

Sonochemical Synthesis of Vaterite-Type Calcium Carbonate Using Steamed Ammonia Liquid Waste without Additives

Xianping Luo,* Xuewen Song,* Chunhua Lai, Jingfeng Wang, and Yuwei Cao

Cite This: *ACS Omega* 2021, 6, 23846−23854

Read Online

ACCESS | Metrics & More | Article Recommendations

ABSTRACT: Herein, metastable spheroidal vaterite calcium carbonate ($CaCO_3$) was prepared using a simple ultrasound technique. The fabricated material comprises an irregular nanoparticle aggregate when steamed ammonia liquid waste, that is, ($CaCl_2$) and $(NH_4)_2CO_3$, is used as the raw material at atmospheric temperature, without any surfactants. The effects of ultrasound amplitude, probe immersion depth, and solution volume on particle properties were investigated. The obtained samples were identified and characterized by X-ray diffraction, Fourier transform infrared spectroscopy, scanning electron microscopy, and the Brunauer−Emmett−Teller technique. Our experiments show that the probe immersion depth and the reaction volume are the key parameters that impact the diameter size and size distribution of the fabricated spheroidal vaterite $CaCO_3$ particles. The ultrasound amplitude considerably affected the particle size and the specific surface area. A possible formation mechanism for pure vaterite is proposed herein, which suggests that simple vaterite $CaCO_3$ is formed owing to the special properties of steamed ammonia liquid waste and the synergistic effects of the ultrasonic system. This study may provide a new method for vaterite $CaCO_3$ synthesis.

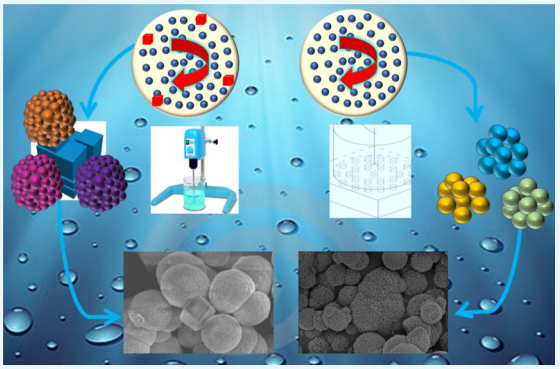

1. INTRODUCTION

Calcium carbonate ($CaCO_3$) is one of the most widely used fill materials. It is used in pigments,[1] plastics,[2] wastewater treatment,[3] paper,[4] cement,[5] rubber, and adhesives.[6] Therefore, synthesizing $CaCO_3$ via a precipitation reaction is a popular topic in chemical engineering. Anhydrous $CaCO_3$ possesses three crystalline polymorphic types (vaterite, aragonite, and calcite), and their thermodynamic stability increases sequentially.[7,8] Because vaterite has the lowest thermodynamic stability, it can easily transform into calcite and/or aragonite via recrystallization when it comes in contact with water.[9−11] Among the polymorphic types, vaterite-phase $CaCO_3$ is expected to have several potential applications in various industries because of its unique properties, such as lower specific gravity, high solubility, high dispersion, large specific surface area, and porous nature, compared with the other two crystalline forms. However, as vaterite can easily transform into more stable calcite and aragonite in an aqueous medium, synthesizing vaterite $CaCO_3$ without additives or a special method is challenging. Therefore, methods to control and obtain vaterite-phase $CaCO_3$ crystals have attracted considerable research attention in recent years.[12−14]

To realize the maximum utilization of $CaCO_3$ in industrial applications, obtaining particles with a fine size, narrow size distribution, and uniform morphology and crystal structure (polymorph) is crucial.[15,16] These properties primarily depend on the synthesis parameters. Several synthesis methods have been used to regulate the crystallization, nucleation, and crystal growth of $CaCO_3$ with the desired properties.[17−19] With the continuous progress in science and technology, a new chemical preparation method has received extensive research attention in the field of $CaCO_3$ synthesis.[20−22] Recently, researchers have found that ultrasound plays a crucial role in the synthesis of inorganic chemicals during some precipitation reactions. While taking advantage of the produced cavitation effect, the ultrasonic chemical method has been widely used to prepare various solid materials.[23,24] Ultrasonochemistry plays an important role in crystallization. For example, ultrasound facilitates the reduction of induction time and/or accelerates the crystal growth of $CaCO_3$ particles during nucleation while eliminating the particle agglomeration width, thus providing better control over particle size distribution, morphology, and physicochemical properties. In addition, ultrasound promotes the precipitation of the different polymorphs of $CaCO_3$.[25,26]

Received: May 27, 2021
Accepted: August 25, 2021
Published: September 4, 2021

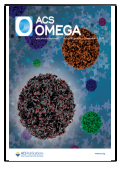

ACS Publications

© 2021 The Authors. Published by American Chemical Society

https://doi.org/10.1021/acsomega.1c02772
ACS Omega 2021, 6, 23846−23854

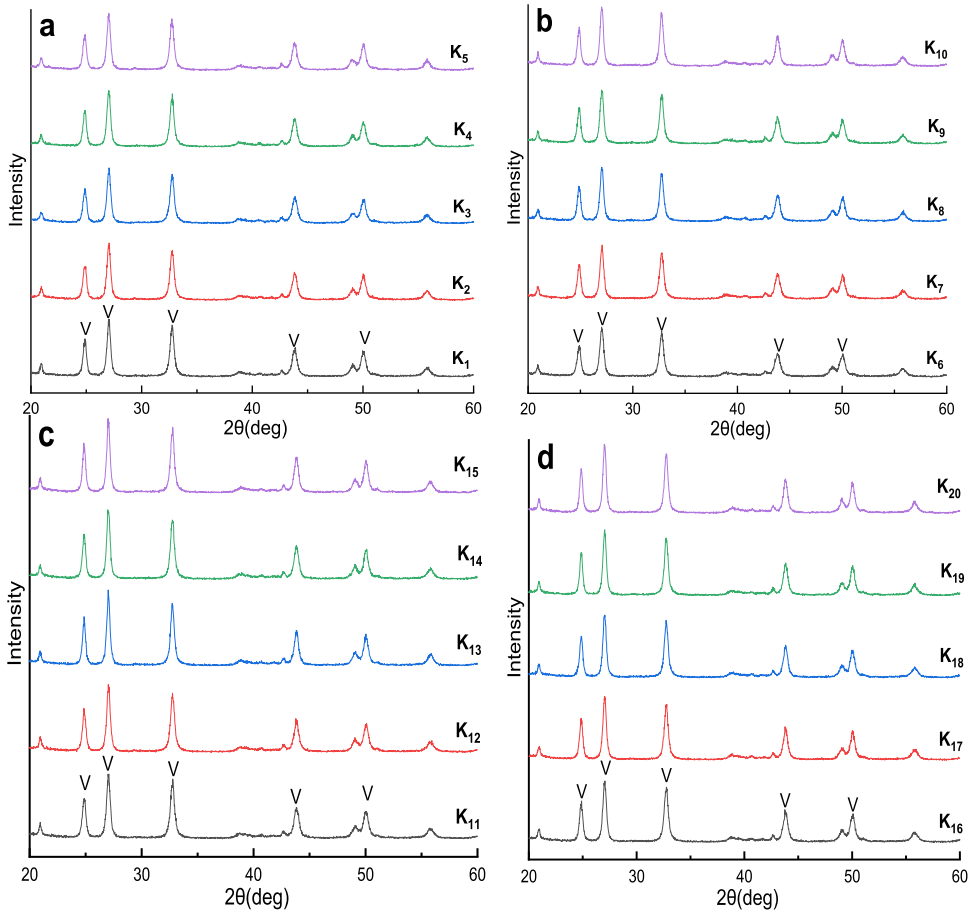

Figure 1. X-ray diffraction (XRD) patterns of $CaCO_3$ crystals prepared using various ultrasonic amplitudes with probe immersion depths and solution volumes of (a) 60 mm and 180 mL, (b) 180 mm and 180 mL, (c) 180 mm and 360 mL, and (d) 180 mm and 540 mL, respectively (V: vaterite).

Therefore, the ultrasound method is commonly used to obtain the desired physicochemical properties of $CaCO_3$ particles.[27,28]

With ease, vaterite can thermodynamically easily transform into the more stable calcite when placed in a water solution;[29] therefore, obtaining vaterite $CaCO_3$ with high-purity crystals is difficult.[30] Some research studies indicated that vaterite can be prepared in the presence of surfactants or via special chemically assisted methods.[31] Recently, several studies have reported the preparation of metastable vaterite by ultrasonic chemically assisted methods. For example, Juhasz-Bortuzzo et al.[32] successfully prepared high-purity vaterite using the ultrasonic technique without any surfactant. Price et al.[33] studied the effects of different ultrasound treatment parameters on the composition of precipitated $CaCO_3$ polymorphs in the absence of an assistant. Kojima et al.[34] investigated the impact of ultrasonic amplitude and frequency on the shape of fabricated vaterite particles in the absence of additives.

Although numerous studies on $CaCO_3$ vaterite polymorphism have been widely carried out, favorable ultrasonic sonochemistry conditions for generating the vaterite polymorph have not been fully identified. Obtaining a fundamental understanding of the correlation between the ultrasonic sonochemistry used and the physicochemical properties of the resulting vaterite product still remains challenging, particularly in the presence of impurity ions with steamed ammonia liquid waste. Herein, the reaction parameters used to prepare vaterite using the ultrasound technique, with steamed ammonia liquid waste and without any surfactants, are evaluated for the first time. The understanding of the physicochemical properties of vaterite $CaCO_3$ synthesized with ultrasonic assistance achieved in this study helps in realizing the large-scale synthesis of high-purity vaterite $CaCO_3$ using steamed ammonia liquid waste as the calcium source.

2. RESULTS AND DISCUSSION

Figure 1 shows the XRD patterns of prepared $CaCO_3$ particles with different ultrasonic amplitudes, probe immersion depths, and solution volume reaction conditions. The XRD results indicate three intensity peaks at 2θ values of 24.92, 26.99, and 32.78° corresponding to *hkl* values of (110), (112), and (114), respectively. XRD results also indicate that all samples obtained under different ultrasound synthesis conditions show pure vaterite (JCPDS: 33-0268) as the only crystalline phase.

The phase composition of the prepared crystalline $CaCO_3$ products under different conditions was further studied by FTIR spectroscopy, as shown in Figure 2. FTIR spectra indicate two characteristic peaks at 872 and 744 cm^{-1}, which are representative of the out-of-plane and in-plane bending modes of CO_3^{2-}, respectively. The FTIR characteristics indicate that pure vaterite was formed for samples undergoing all ultrasonic preparation conditions.

Based on the XRD patterns and FTIR spectra, only the vaterite-phase $CaCO_3$ was obtained via sonochemical synthesis

https://doi.org/10.1021/acsomega.1c02772
ACS Omega 2021, 6, 23846−23854

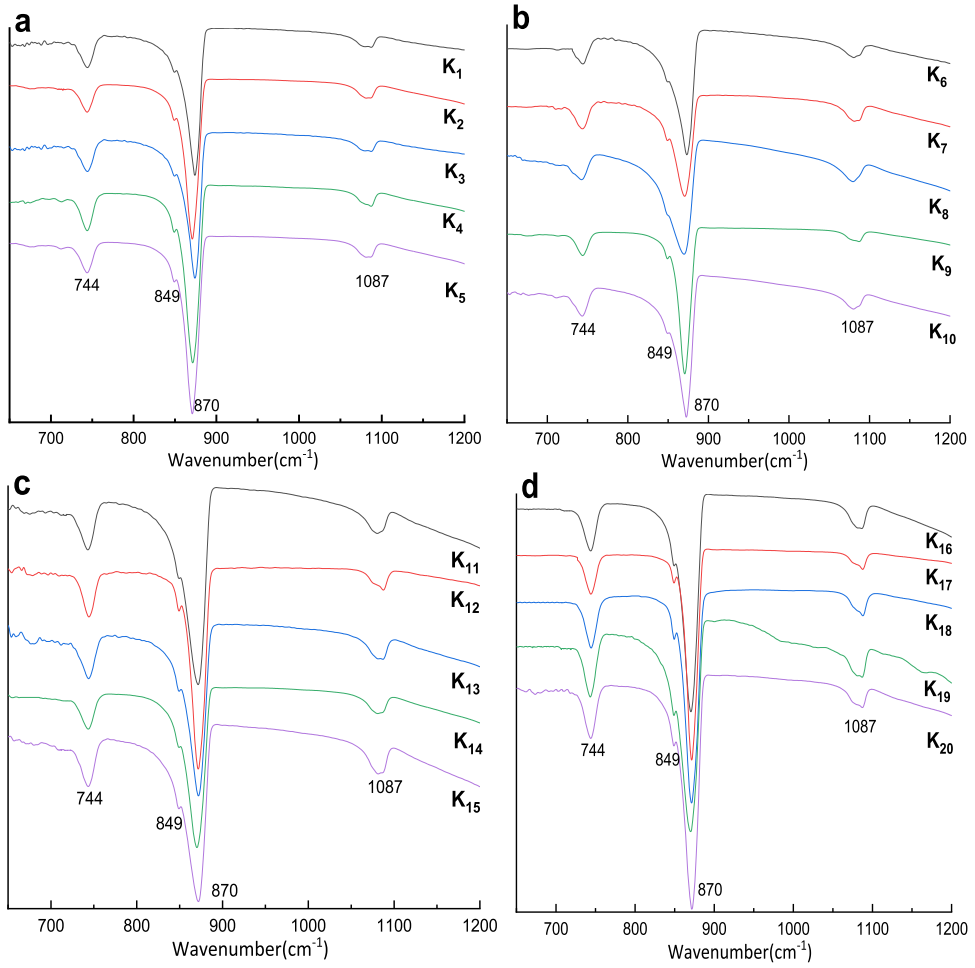

Figure 2. Fourier transform infrared (FTIR) spectra of $CaCO_3$ prepared using various ultrasonic amplitudes with probe immersion depths and solution volumes of (a) 60 mm and 180 mL, (b) 180 mm and 180 mL, (c) 180 mm and 360 mL, and (d) 180 mm and 540 mL, respectively.

using steamed ammonia liquid waste as the calcium source and in the absence of additives. The results also show that the ultrasound amplitude, probe immersion depth, and solution volume have no effect on the crystal phase composition of the prepared products. This method can realize single metastable spherical vaterite $CaCO_3$. Our previous research studies[35−37] have shown that preparing single-purity metastable vaterite $CaCO_3$ through conventional simple mechanical mixing using steamed ammonia liquid waste as the calcium source is difficult. In addition, several reported studies have also indicated that achieving single-phase high-purity vaterite $CaCO_3$ without additives[38−40] is difficult even when using the ultrasonic chemistry method.[41] Therefore, it can be concluded that by using steam ammonia liquid waste as the raw calcium source, vaterite can be effectively prepared using ultrasonic waves.

The morphologies of products obtained under different probe depths, solution volumes, and ultrasonic amplitudes were characterized by scanning electron microscopy (SEM) (Figures 3 and 4). The SEM images show that all vaterite samples exhibit spherical and fine-grained morphologies. Figure 3 (K_5 and K_{10}) and Figure 4 (K_{15} and K_{20}) show that the spheroidal vaterite samples are composed of an agglomeration of particles tens of nanometers in size, and the high-magnification SEM images can further verify these conclusions. The vaterite products prepared under the action of ultrasound show many agglomerations (Figures 3 and 4), and the particle size and morphology of the resulting products exhibit only minor alterations. When the ultrasonic amplitude is increased, the agglomeration degree of the products reduces to a certain extent. From Figures 3 and 4, it can be seen that the vaterite aggregates produced using the ultrasonic method are inconsistent with those obtained by the author in relevant studies.[36−38] Therefore, it can be concluded that the ultrasonic method can prevent vaterite agglomeration.

Table 1 and Figure 5 show the changes in the average diameter (D_{50}) and particle size distribution with a change in the ultrasonic amplitude. Table 1 shows that the sample vaterite size decreased with an increase in the ultrasonic amplitude. The D_{50} particle size of K_1−K_5 samples decreased from 4.80 to 3.18 μm, and the standard deviation of the D_{50} size of these five samples was 0.5752. The D_{50} particle size of K_6−K_{10} samples decreased from 5.66 to 3.88 μm, and the standard deviation of the D_{50} size of these five samples was 0.7321. The D_{50} particle size of K_{11}−K_{15} samples decreased from 7.11 to 4.62 μm, and the standard deviation of the D_{50} size of these five samples was 0.8788. Moreover, the D50 particle size of K_{15}−K_{20} decreased from 5.88 to 2.78 μm, and the standard deviation of the D_{50} size of these five samples was 1.0660. For K_1−K_{20} samples, when the ultrasonic probe depth and the reaction volume increased, the effect of the change in

https://doi.org/10.1021/acsomega.1c02772
ACS Omega 2021, 6, 23846−23854

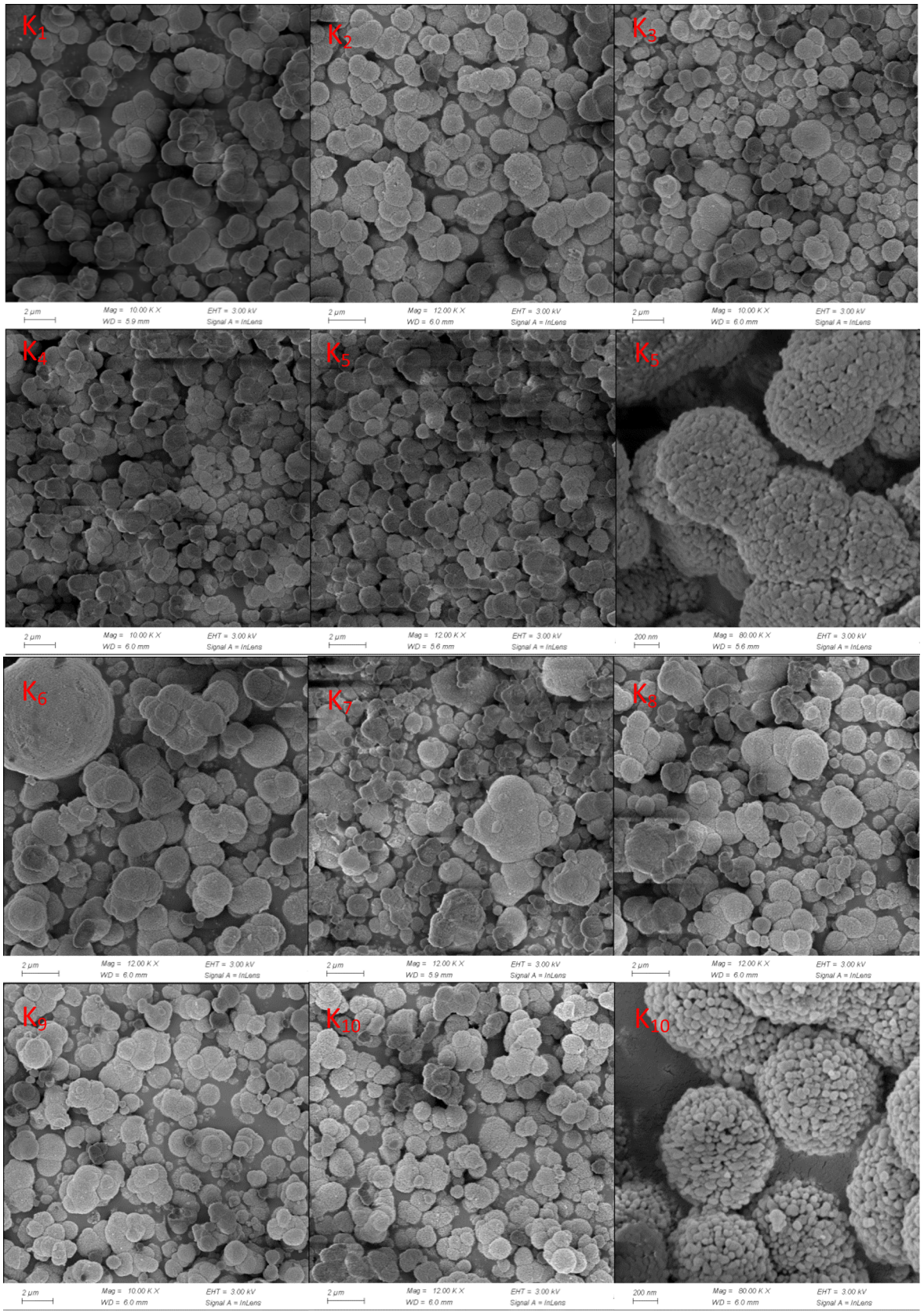

Figure 3. Morphologies of vaterite $CaCO_3$ obtained using different ultrasonic amplitudes, probe immersion depths, and solution volumes of (K_1–K_5) 60 mm and 180 mL and (K_6–K_{10}) 180 mm and 180 mL.

the ultrasonic amplitude on the change of the product particle size increased.

Table 1 shows that as the ultrasonic amplitude increased, the particle size of the vaterite products decreased. Figure 4 shows

https://doi.org/10.1021/acsomega.1c02772
ACS Omega 2021, 6, 23846−23854

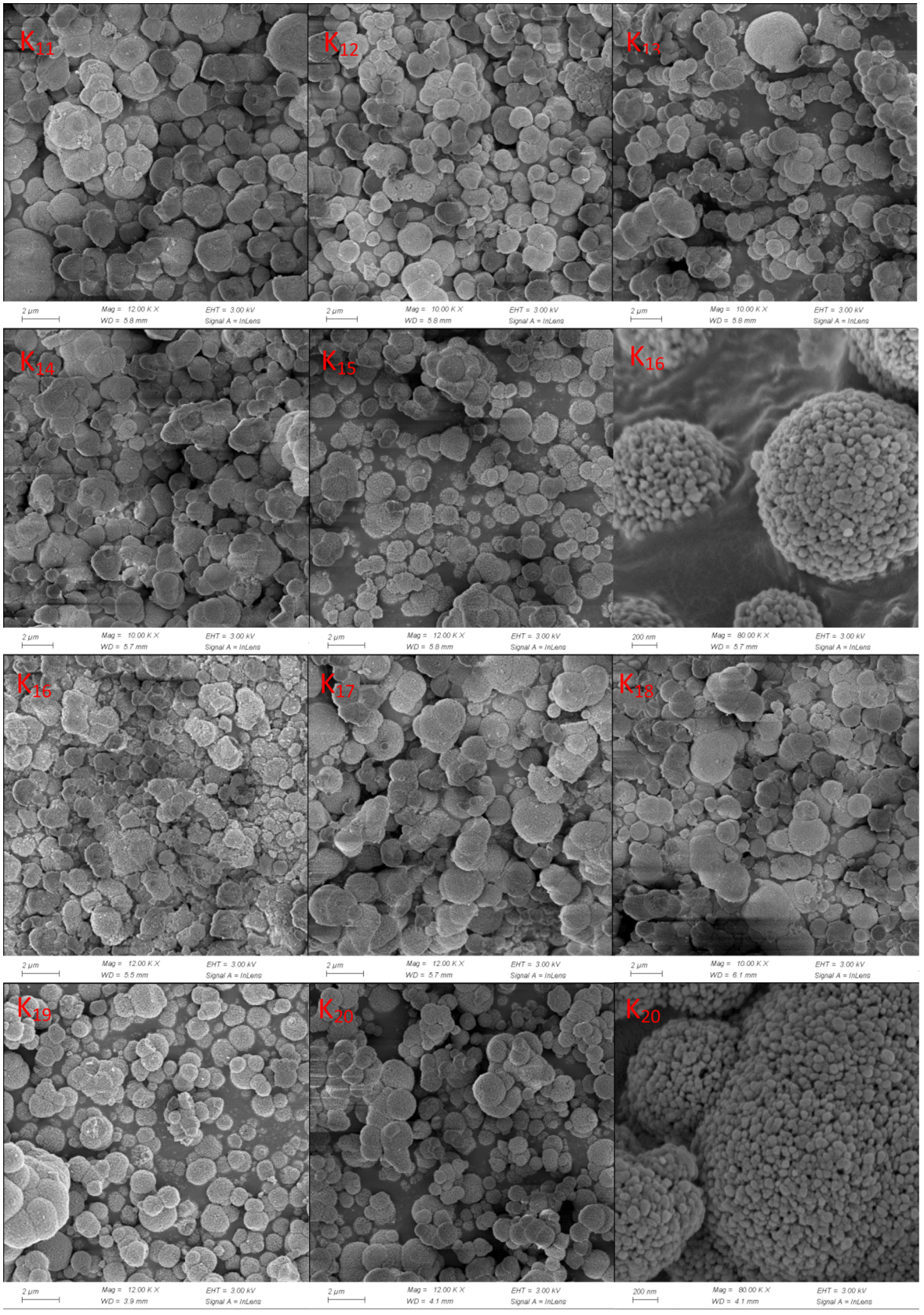

Figure 4. Morphologies of vaterite $CaCO_3$ obtained using different ultrasonic amplitudes, probe immersion depths, and solution volumes of (K_{11}–K_{15}) 180 mm and 360 mL and (K_{16}–K_{20}) 180 mm and 540 mL.

that as the ultrasonic amplitude increased, the product reunion decreased; thus, the particle size of the winning product decreased. Thus, increasing the ultrasonic amplitude can reduce the size of the vaterite particles. Figure 5 shows that

https://doi.org/10.1021/acsomega.1c02772
ACS Omega 2021, 6, 23846−23854

Table 1. D_{50} Size of Vaterite Obtained under Different Preparation Conditions

samples	K_1	K_2	K_3	K_4	K_5	K_6	K_7	K_8	K_9	K_{10}
D_{50} (μm)	4.80	4.67	4.04	4.06	3.18	5.66	4.83	4.69	4.51	3.38
samples	K_{11}	K_{12}	K_{13}	K_{14}	K_{15}	K_{16}	K_{17}	K_{18}	K_{19}	K_{20}
D_{50} (μm)	7.11	6.18	5.29	5.14	4.62	5.88	5.21	4.44	3.93	2.78

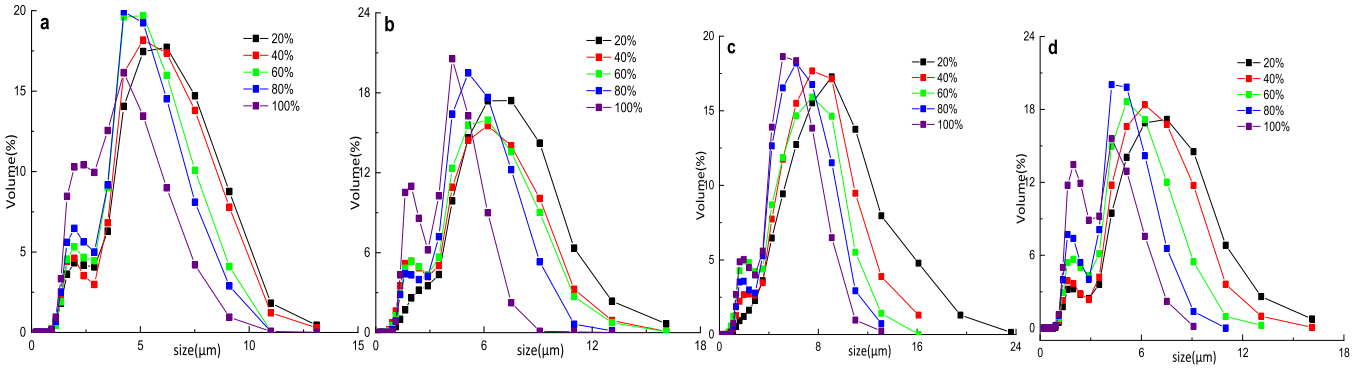

Figure 5. Particle diameter distribution of samples prepared using various ultrasonic amplitudes, probe immersion depths, and solution volumes of (a) 60 mm and 180 mL, (b) 180 mm and 180 mL, (c) 180 mm and 360 mL, and (d) 180 mm and 540 mL.

the size distribution of the resultant vaterite decreased from 20 to 100% as the ultrasonic amplitude increased. From Figure 5, it is observed that the vaterite size distribution is bimodal with two optimum volumes. The possible mechanism of this phenomenon is Oswald ripening. The particle size of vaterite formed after crystal nucleation is 1−3 μm, and a portion of the vaterite gathered together the particles owing to Oswald maturation when the reaction time was increased; hence, the particle size increased to 5−18 μm. Therefore, the product contains both small unaggregated particles and large aggregated particles, resulting in a bimodal particle size distribution pattern. The resultant product is composed of many agglomerates and some agglomerated particles, as shown in the SEM images in Figures 3 and 4, providing a basis for the results obtained using a laser particle size analyzer (LPSA) in Figure 5. Therefore, the size distribution of the vaterite sample is bimodal with two optimum volumes.

Table 2 shows the specific surface areas of different products obtained using the BET method. The results in Table 2 show

Table 2. Brunauer−Emmett−Teller (BET) Surface Area of Vaterite Obtained under Different Preparation Conditions

samples	K_1	K_2	K_3	K_4	K_5
specific surface area (m^2/g)	12.27	13.88	13.64	16.36	20.91
samples	K_6	K_7	K_8	K_9	K_{10}
specific surface area (m^2/g)	6.75	13.56	11.07	10.36	16.47
samples	K_{11}	K_{12}	K_{13}	K_{14}	K_{15}
specific surface area (m^2/g)	11.05	10.56	11.29	12.62	15.08
samples	K_{16}	K_{17}	K_{18}	K_{19}	K_{20}
specific surface area (m^2/g)	14.95	16.19	15.10	16.56	18.20

that when the ultrasonic amplitude was increased, the specific surface area of the prepared products increased. When the ultrasonic amplitude was increased from 20 to 100%, the specific surface area of the vaterite samples showed an increasing trend and rapid enlargement, from the initial value of 12.27 to 20.91 m^2/g at a probe immersion depth of 60 mm and a solution volume of 180 mL. The specific surface areas increased from 6.75 m^2/g at 20% ultrasonic amplitude to 16.47 m^2/g at 100% ultrasonic amplitude at a probe immersion depth of 180 mm and a solution volume of 180 mL. At a probe immersion depth of 180 mm and a solution volume of 360 mL, the specific surface area increased from 11.05 to 15.08 m^2/g when the ultrasonic amplitude was increased from 20 to 100%. At a probe immersion depth of 180 mm and a solution volume of 540 mL, the specific surface area increased from 14.95 to 18.02 m^2/g with an increase in the ultrasonic amplitude from 20 to 100%. When comparing the specific surface areas of K_1−K_{10} samples, it can be seen that as the probe depth increased, the specific surface area of the prepared product decreased slightly. However, when comparing the specific surface areas of K_5−K_{20} samples, it can be seen that the specific surface area of the prepared product increased with an increase in the reaction volume.

The above characterization results indicate that pure metastable vaterite was prepared using a simple ultrasonic chemistry method without additives and by using steamed ammonia liquid waste as the calcium source. The formation of vaterite $CaCO_3$ appears to have two main functions. Table 3

Table 3. Content of Main Impurity Ions in Steamed Ammonia Liquid Waste

ions	concentration (mol/L)
K^+	0.014
Na^+	0.054
Mg^{2+}	0.0000058

indicates that a small amount of Mg^{2+}, K^+, and Na^+ is present in the steamed ammonia liquid waste. Several literature studies have reported that Mg^{2+}, K^+, and Na^+ can change the crystallization process of $CaCO_3$;[42−44] therefore, metastable vaterite is formed owing to the steamed ammonia liquid waste.[45] Second, our previous research studies[35−38] have shown that it is difficult to prepare single-phase high-purity metastable vaterite $CaCO_3$ by conventional simple mechanical mixing using steamed ammonia liquid waste as the calcium source. However, the current study indicates that pure vaterite $CaCO_3$ is obtained using the ultrasonic chemistry method

https://doi.org/10.1021/acsomega.1c02772
ACS Omega 2021, 6, 23846−23854

when steamed ammonia liquid waste is employed. Hence, it can be explained that the ultrasonic reaction played a decisive role in the formation of vaterite.

Results from the study by Dzakula et al.[46] indicate that the ultrasound treatment resulted in a decrease of induction period in the precipitation systems, and the formation of vaterite particles occurs within the initial reaction stage. Combined with the literature data,[47,48] it can be suggested that the most important mechanism responsible for the promotion of vaterite formation under ultrasonic irradiation is supposed to be ultrasonic cavitation. Under conventional conditions, the formed vaterite undergoes a phase change to form a more stable calcite according to the literature study. Wagterveld et al.[49] suggested that cavitation generated by ultrasound can induce micromixing and/or shear/stress. Our research suggested[50] that a high stirring speed can strongly prevent the vaterite transition to calcite. Hence, this research suggested that ultrasonic chemistry can inhibit the vaterite transformation to a more thermodynamically stable aragonite and calcite, thus promoting the formation of pure vaterite $CaCO_3$ products. Based on the experimental results and the above analysis, it is inferred that the ultrasonic reaction for the promotion of vaterite formation can prevent the phase transition of vaterite and allow the vaterite product to remain stable in the reaction system.

3. CONCLUSIONS

We obtained pure vaterite $CaCO_3$ particles using steamed ammonia liquid waste as the calcium source and without additives via sonochemical synthesis. Vaterite-phase $CaCO_3$ with typical spherical particles of 2.78 μm can be prepared, and the BET surface area was 20.91 m^2/g at 100% ultrasound amplitude. The effects of the ultrasound amplitude, probe immersion depth, and solution volume on the size, particle size distribution, and specific surface area of the vaterite samples were investigated. With an increase in the ultrasound amplitude, the product particle size decreased while the specific surface area increased. The ultrasonic amplitude, probing depth, and solution volume clearly have an influence on the particle size and specific surface area of the final vaterite product. We used industrial waste (steamed ammonia liquid waste) to realize metastable vaterite via facile precipitation using sonochemical synthesis without any other assistance. This method is likely to realize large-scale industrial applications owing to the lack of template-directed or additive-assisted conditions in the preparation process.

4. EXPERIMENTAL SECTION

4.1. Materials. Steamed ammonia liquid waste was provided by Qinghai West Magnesium Industry Co., Ltd. Filtration was used to remove solid impurities. The subnatant was collected as the calcium ($CaCl_2$) source via three filtration processes. Ammonium carbonate ($(NH_4)_2CO_3$) was acquired from Tianjin Bodi Chemical Reagent Company. All chemical reagents were of analytical grade.

4.2. Synthetic Conditions. Vaterite was prepared via facile precipitation in glass bottles using the ultrasonic chemical method. Ultrasound waves were generated using an ultrasonic homogenizer (OuHor UH2000-T) on which a horn with a diameter of 12 mm was mounted. The ultrasound amplitude of the sonication treatment could be set using a controller. A frequency of 24.5 kHz and a power of 1200 W were used during the experiments. A 0.60 mol/L $CaCl_2$ aqueous solution of steamed ammonia liquid waste was used as the stock solution. A solution of 0.60 mol/L $(NH_4)_2CO_3$ was dissolved in water; the weighed $(NH_4)_2CO_3$ was placed in deionized water for synthesis. For particle preparation, 0.60 mol/L $CaCl_2$ and 0.60 mol/L $(NH_4)_2CO_3$ solutions were immediately poured into glass vessels. The ultrasound amplitudes were 20, 40, 60, 80, and 100%. The mixed solution was uniformly sonically oscillated for 10 min. Table 4 shows the preparation conditions for each experiment. When the reaction was completed, the obtained $CaCO_3$ product was collected using a suction filtration device, and the particles were washed with deionized water several times during the filtration process. Finally, to detect and characterize the obtained samples, they were placed in a desiccator and dried at 105 °C for 12 h.

Table 4. Experimental Parameters for Producing Vaterite

samples	ultrasonic amplitude (%)	probe immersion depth (mm)	solution volume (mL)
K_1	20	60	180
K_2	40	60	180
K_3	60	60	180
K_4	80	60	180
K_5	100	60	180
K_6	20	180	180
K_7	40	180	180
K_8	60	180	180
K_9	80	180	180
K_{10}	100	180	180
K_{11}	20	180	360
K_{12}	40	180	360
K_{13}	60	180	360
K_{14}	80	180	360
K_{15}	100	180	360
K_{16}	20	180	540
K_{17}	40	180	540
K_{18}	60	180	540
K_{19}	80	180	540
K_{20}	100	180	540

4.3. Characterization. Powder XRD (DX-2700BH) and FTIR (Cary 630) were used to identify the phases of the resultant powders. The crystalline phase of the resultant particles was determined by XRD using Cu Kα radiation (1.54184 Å) and a step length of 0.02°. The morphology and size of the particles were determined using a SEM (ZEISS Gemini 300). A gold film was sputtered on the particles placed on the glass slide, and the sample was examined at a 3 kV accelerating voltage. The specific surface area and the pore size of $CaCO_3$ were measured using N_2 adsorption−desorption isotherm (ASAP2460) measurements; particles were degassed overnight at 180 °C before the measurement. The pore size distribution and the specific surface area were determined using Barrett−Joyner−Halenda and BET methods, respectively. The average $CaCO_3$ particle size and distribution were measured using an LPSA (OMCC SCF-106A) by employing the dynamic light scattering method. The impurity ion content of the steamed ammonia liquid waste was measured using an inductively coupled plasma atomic emission spectrometer (740 0radial, IC74RA0097).

https://doi.org/10.1021/acsomega.1c02772
ACS Omega 2021, 6, 23846−23854

AUTHOR INFORMATION

Corresponding Authors

Xianping Luo − *Jiangxi Key Laboratory of Mining & Metallurgy Environmental Pollution Control, Jiangxi University of Science and Technology, Ganzhou 341000, China; College of Material Science and Engineering, Xi'an University of Architecture and Technology, Xi'an 710055, China; Western Mining Group Technology Development Co. Ltd., Western Mining Group Co., Ltd., Xining 810001, China*; Email: luoxianping9491@163.com

Xuewen Song − *Jiangxi Key Laboratory of Mining & Metallurgy Environmental Pollution Control, Jiangxi University of Science and Technology, Ganzhou 341000, China; College of Material Science and Engineering, Xi'an University of Architecture and Technology, Xi'an 710055, China*; orcid.org/0000-0001-9438-6167; Email: Songxwhl@163.com

Authors

Chunhua Lai − *Western Mining Group Technology Development Co. Ltd., Western Mining Group Co., Ltd., Xining 810001, China*

Jingfeng Wang − *Western Mining Group Technology Development Co. Ltd., Western Mining Group Co., Ltd., Xining 810001, China*

Yuwei Cao − *Western Mining Group Technology Development Co. Ltd., Western Mining Group Co., Ltd., Xining 810001, China*

Complete contact information is available at: https://pubs.acs.org/10.1021/acsomega.1c02772

Notes

The authors declare no competing financial interest.

ACKNOWLEDGMENTS

This work was partially supported by the National Key Research and Development Program of China (2018YFC1903805) and the Major Science and Technology Projects of Qinghai Province (2020-GX-A1).

REFERENCES

(1) Karakaş, F.; Vaziri Hassas, B.; Çelik, M. S. Effect of precipitated calcium carbonate additions on waterborne paints at different pigment volume concentrations. *Prog. Org. Coat.* **2015**, *83*, 64−70.

(2) de Oliveira, A. G.; Moreno, J. F.; de Sousa, A. M. F.; Escócio, V.; de Oliveira Cavalcanti Guimarães, M. J.; da Silva, A. L. N. Composites based on high-density polyethylene, polylactide and calcium carbonate: effect of calcium carbonate nanoparticles as co-compatibilizers. *Polym. Bull.* **2020**, *77*, 2889−2904.

(3) Zhou, L. S.; Peng, T. J.; Sun, H. J.; Guo, X. G.; Fu, D. The Characterization and Amoxicillin Adsorption Activity of Mesopore $CaCO_3$ Microparticles Prepared Using Rape Flower Pollen. *Minerals* **2019**, *9*, 254.

(4) Kuusisto, J.; Tiittanen, T.; Maloney, T. C. Property optimization of calcium carbonate precipitated in a high shear, circulation reactor. *Powder Technol.* **2016**, *303*, 241−250.

(5) Cao, M. L.; Khan, M.; Ahmed, S. Effectiveness of Calcium Carbonate Whisker in Cementitious Composites. *Period. Polytech. Civil. Eng.* **2020**, *64*, 265−275.

(6) Said, A.; Mattila, H. P.; Järvinen, M.; Zevenhoven, R. Production of precipitated calcium carbonate (PCC) from steelmaking slag for fixation of CO_2. *Appl. Energy* **2013**, *112*, 765−771.

(7) Tomioka, T.; Fuji, M.; Takahashi, M.; Takai, C.; Utsuno, M. Hollow Structure Formation Mechanism of Calcium Carbonate Particles Synthesized by the CO_2 Bubbling Method. *Cryst. Growth Des.* **2012**, *12*, 771−776.

(8) Nagaraja, A. T.; Pradhan, S.; McShane, M. J. Poly(vinylsulfonic acid) assisted synthesis of aqueous solution stable vaterite calcium carbonate nanoparticles. *J. Colloid Interface Sci.* **2014**, *418*, 366−372.

(9) Sarkar, A.; Dutta, K.; Mahapatra, S. Polymorph Control of Calcium Carbonate Using Insoluble Layered Double Hydroxide. *Cryst. Growth Des.* **2013**, *13*, 204−211.

(10) Cherkas, O.; Beuvier, T.; Breiby, D. W.; Chushkin, Y.; Zontone, F.; Gibaud, A. Direct Observation of Microparticle Porosity Changes in Solid-State Vaterite to Calcite Transformation by Coherent X-ray Diffraction Imaging. *Cryst. Growth Des.* **2017**, *17*, 4183−4188.

(11) Zhao, Y. Y.; du, W.; Sun, L. M.; Yu, L.; Jiao, J. J.; Wang, R. Facile synthesis of calcium carbonate with an absolutely pure crystal form using 1-butyl-3-methylimidazolium dodecyl sulfate as the modifier. *Colloid Polym. Sci.* **2013**, *291*, 2191−2202.

(12) Zhang, Z.; Yang, B. J.; Tang, H. W.; Chen, Z. L.; Wang, B. High-yield synthesis of vaterite $CaCO_3$ microspheres in ethanol/water: structural characterization and formation mechanisms. *J. Mater. Sci.* **2015**, *50*, 5540−5548.

(13) Zheng, T. W.; Zhang, X.; Yi, H. H. Spherical vaterite microspheres of calcium carbonate synthesized with poly(acrylic acid) and sodium dodecyl benzene sulfonate. *J. Cryst. Growth* **2019**, *528*, No. 125275.

(14) Pérez-Villarejo, L.; Takabait, F.; Mahtout, L.; Carrasco-Hurtado, B.; Eliche-Quesada, D.; Sánchez-Soto, P. J. Synthesis of vaterite $CaCO_3$ as submicron and nanosized particles using inorganic precursors and sucrose in aqueous medium. *Ceram. Int.* **2018**, *44*, 5291−5296.

(15) Bang, J. H.; Jang, Y. N.; Kim, W. B.; Song, K. S.; Jeon, C. W.; Chae, S. C.; Lee, S. W.; Park, S. J.; Lee, M. G. Specific surface area and particle size of calcium carbonate precipitated by carbon dioxide microbubbles. *Chem. Eng. J.* **2012**, *198-199*, 254−260.

(16) Sha, F.; Zhu, N.; Bai, Y. J.; Li, Q.; Guo, B.; Zhao, T. X.; Zhang, F. J.; Zhang, B. Controllable Synthesis of Various $CaCO_3$ Morphologies Based on a CCUS Idea. *ACS Sustain. Chem. Eng.* **2016**, *4*, 3032−3044.

(17) Arifin, Z.; Triwikantoro; Subagyo, B. A.; Zainuri, M.; Darminto, D. Synthesis of Precipitate Calcium Carbonate with Variation Morphology from Limestone by Using Solution Mixing Method. *Mater. Sci. Forum* **2019**, *966*, 200−203.

(18) Miyazaki, T.; Arii, T.; Shirosaki, Y. Control of crystalline phase and morphology of calcium carbonate by electrolysis: Effects of current and temperature. *Ceram. Int.* **2019**, *45*, 14039−14044.

(19) Dang, H. C.; Xu, Z. Z.; Chen, Z. S.; Wu, W. L.; Feng, J.; Sun, Y. Y.; Jin, F. C.; Li, J.; Ge, F. A Facile and Controllable Method to In Situ Synthesize Stable Hydrophobic Vaterite Particles. *Cryst. Res. Technol.* **2019**, *54*, No. 1800243.

(20) Gedanken, A. Using sonochemistry for the fabrication of nanomaterials. *Ultrason. Sonochem.* **2004**, *11*, 47−55.

(21) Alavi, M. A.; Morsali, A. Syntheses and characterization of Mg $(OH)_2$ and MgO nanostructures by ultrasonic method. *Ultrason. Sonochem.* **2010**, *17*, 441−446.

(22) Tang, X. J.; Nie, Y. X.; Jin, Q.; Guo, L.; Zhao, J.; Li, T.; Zhu, Y. M. Kinetics and mechanism of ultrasonic-assisted magnesium oxide hydration. *Ultrason. Sonochem.* **2018**, *40*, 995−1002.

(23) Song, G. L.; Ma, S. D.; Tang, G. Y.; Wang, X. W. Ultrasonic-assisted synthesis of hydrophobic magnesium hydroxide nanoparticles. *Colloids Surf. A: Physicochem. Eng. Asp.* **2010**, *364*, 99−104.

(24) Shu-Yu, W.; Wen-Zhi, H.; Chang, L.; Guang-Ming, L.; Fei-Er, Z. Characterizations and preparation of Mg $(OH)_2$ nanocrystals through ultrasonic-hydrothermal route. *Res. Chem. Intermed.* **2016**, *42*, 4135−4145.

(25) Wang, B.; Pan, Z. H.; Cheng, H. G.; Chen, Z. L.; Cheng, F. Q. High-yield synthesis of vaterite microparticles in gypsum suspension system via ultrasonic probe vibration/magnetic stirring. *J. Cryst. Growth* **2018**, *492*, 122−131.

(26) Cheng, H. G.; Wang, X.; Wang, B.; Zhao, J.; Liu, Y.; Cheng, F. Q. Effect of ultrasound on the morphology of the $CaCO_3$ precipitated

from $CaSO_4$-NH_3-CO_2-H_2O system. *J. Cryst. Growth* **2017**, *469*, 97−105.
(27) Nishida, I. Precipitation of calcium carbonate by ultrasonic irradiation. *Ultrason. Sonochem.* **2004**, *11*, 423−428.
(28) López-Periago, A. M.; Pacciani, R. L.; Vega, F.; Domingo, C. Monitoring the Effect of Mineral Precursor, Fluid Phase CO_2·H_2O Composition, and Stirring on $CaCO_3$ Crystallization in a Supercritical-Ultrasound Carbonation Process. *Cryst. Growth Des.* **2011**, *11*, 5324−5332.
(29) Flaten, E. M.; Seiersten, M. J.; Andreassen, J.-P. Polymorphism and morphology of calcium carbonate precipitated in mixed solvents of ethylene glycol and water. *J. Cryst. Growth* **2009**, *311*, 3533−3538.
(30) Kabalah-Amitai, J. L.; Mayzel, B.; Kauffmann, Y.; Fitch, A. N.; Bloch, L.; Gilbert, P. U. P. A.; Pokroy, B. Vaterite crystals contain two interspersed crystal structures. *Science* **2013**, *340*, 454−457.
(31) Corvisier, J.; Brunet, F.; Fabbri, A.; Bernard, S.; Findling, N.; Rimmelé, G.; Barlet-Gouédard, V.; Beyssac, O.; Goffé, B. Raman mapping and numerical simulation of calcium carbonates distribution in experimentally carbonated Portland-cement cores. *Eur. J. Mineral.* **2010**, *22*, 63−74.
(32) Juhasz-Bortuzzo, J. A.; Myszka, B.; Silva, R.; Boccaccini, A. R. Sonosynthesis of Vaterite-Type Calcium Carbonate. *Cryst. Growth Des.* **2017**, *17*, 2351−2356.
(33) Price, G. J.; Mahon, M. F.; Shannon, J.; Cooper, C. Composition of Calcium Carbonate Polymorphs Precipitated Using Ultrasound. *Cryst. Growth Des.* **2011**, *11*, 39−44.
(34) Kojima, Y.; Yamaguchi, K.; Nishimiya, N. Effect of amplitude and frequency of ultrasonic irradiation on morphological characteristics control of calcium carbonate. *Ultrason. Sonochem.* **2010**, *17*, 617−620.
(35) Luo, X. P.; Song, X. W.; Cao, Y. W.; Song, L.; Bu, X. Z. Investigation of calcium carbonate synthesized by steamed ammonia liquid waste without use of additives. *RSC Adv.* **2020**, *10*, 7976−7986.
(36) Song, X. W.; Zhang, L.; Cao, Y. W.; Zhu, J. H.; Luo, X. P. Effect of pH and temperatures on the fast precipitation vaterite particle size and polymorph stability without additives by steamed ammonia liquid waste. *Powder Technol.* **2020**, *374*, 263−273.
(37) Song, X. W.; Cao, Y. W.; Bu, X. Z.; Luo, X. P. Porous Vaterite and Cubic Calcite Aggregated Calcium Carbonate Obtained from Steamed Ammonia Liquid Waste for Cu^{2+} Heavy Metal Ions Removal by Adsorption Process. *Appl. Surf. Sci.* **2021**, *536*, No. 147958.
(38) Wang, X. H.; Sun, X. Y.; Zhang, Q.; Marchetti, A.; Wu, L.; Guan, Y. B. Hierarchical pine-dendritic vaterite preparation and micropatterning with microwave technique. *Mater. Lett.* **2017**, *208*, 39−42.
(39) Zhao, T. X.; Guo, B.; Zhang, F.; Sha, F.; Li, Q.; Zhang, J. B. Morphology Control in the Synthesis of $CaCO_3$ Microspheres with a Novel CO_2-Storage Material. *ACS Appl. Mater. Interfaces* **2015**, *7*, 15918−15927.
(40) Oral, Ç. M.; Ercan, B. Influence of pH on morphology, size and polymorph of room temperature synthesized calcium carbonate particles. *Powder Technol.* **2018**, *339*, 781−788.
(41) Polat, S.; Sayan, P. Ultrasonic-assisted eggshell extract-mediated polymorphic transformation of calcium carbonate. *Ultrason. Sonochem.* **2020**, *66*, No. 105093.
(42) Han, Y.; Zhang, C. X.; Wu, L. C.; Zhang, Q. R.; Zhu, L.; Zhao, R. K. Influence of alternating electromagnetic field and ultrasonic on calcium carbonate crystallization in the presence of magnesium ions. *J. Cryst. Growth* **2018**, *499*, 67−76.
(43) Zhang, J.; Dong, C. H.; Sun, Y. Z.; Yu, J. G. Mechanism of Magnesium's Influence on Calcium Carbonate Crystallization: Kinetically Controlled Multistep Crystallization. *Cryst. Res. Technol.* **2018**, *53*, No. 1800075.
(44) Mejri, W.; Ben Salah, I.; Tlili, M. M. Speciation of Fe (II) and Fe(III) effect on CaCO3 crystallization. *Cryst. Res. Technol.* **2015**, *50*, 236−243.
(45) Trushina, D. B.; Bukreeva, T. V.; Kovalchuk, M. V.; Antipina, M. N. $CaCO_3$ vaterite microparticles for biomedical and personal care applications. *Mater. Sci. Eng. C* **2014**, *45*, 644−658.
(46) Njegić Džakula, B.; Kontrec, J.; Ukrainczyk, M.; Sviben, S.; Kralj, D. Polymorphic composition and morphology of calcium carbonate as a function of ultrasonic irradiation. *Cryst. Res. Technol.* **2014**, *49*, 244−256.
(47) Kirboga, S.; Oner, M.; Akyol, E. The effect of ultrasonication on calcium carbonate crystallization in the presence of biopolymer. *J. Cryst. Growth* **2014**, *401*, 266−270.
(48) Svenskaya, Y. L.; Fattah, H.; Zakharevich, A. M.; Gorin, D. A.; Sukhorukov, G. B.; Parakhonskiy, B. V. Ultrasonically assisted fabrication of vaterite submicron-sized carriers. *Adv. Powder Technol.* **2016**, *27*, 618−624.
(49) Wagterveld, M. R.; Miedema, H.; Witkamp, G. J. Effect of Ultrasonic Treatment on Early Growth during $CaCO_3$ Precipitation. *Cryst. Growth Des.* **2012**, *12*, 4403−4410.
(50) Song, X. W.; Weng, C. J.; Cao, Y. W.; Kong, H. M.; Luo, X. P. Facile synthesis of pure vaterite using steamed ammonia liquid waste and ammonium carbonate without additives via simple mechanical mixing. *Powder Technol.* **2021**, *386*, 361−371.

https://doi.org/10.1021/acsomega.1c02772
ACS Omega 2021, 6, 23846−23854